Second forerunners in reflection and transmission data

Egorov, Igor

1998

CODEN:LUTEDX/(TEAT-7071)/1-16/(1998)

Revision No. 1: April 1998

Second forerunners in reflection and transmission data

Igor Egorov

Department of Electroscience
Electromagnetic Theory
Lund Institute of Technology
Sweden

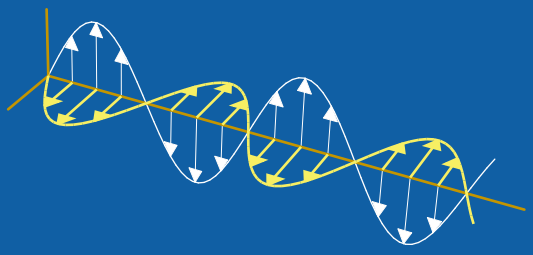

Igor Egorov

Department of Electroscience
Electromagnetic Theory
Lund Institute of Technology
P.O. Box 118
SE-221 00 Lund
Sweden

Editor: Gerhard Kristensson

Abstract

Second forerunner approximations to the transmission and reflection kernels for a temporally dispersive, nonmagnetic, isotropic slab are obtained. Numerical results are presented for two different dispersion models and are compared with the second forerunner approximations. Finally, transmission and reflection kernels are used to reconstruct the first susceptibility moments of the material of the slab.

1 Introduction

The dynamics of a signal propagating through a temporally dispersive, nonmagnetic, simple (linear, homogeneous, and isotropic) medium is a subject that has been studied extensively in electromagnetic field analysis [1–3, 6, 9, 12, 14]. A temporally dispersive medium is characterized by the property that propagating pulses change their shape. This change is due to the fact that different spectral components of the signal are propagating with different phase velocities and are attenuated at different rates. All real materials of any interest are temporally dispersive; therefore, the mentioned effects, generally, cannot be neglected unless the analyzed signal is monochromatic.

The characteristic property of pulse propagation in a temporally dispersive material is the presence of special transient fields — forerunners (precursors). The first (Sommerfeld) forerunner represents the leading-edge behavior of the propagating pulse and is usually characterized by high frequencies and large amplitudes. The second (Brillouin) forerunner arrives after the first one and constitutes a sudden significant rise in amplitude. It is due to the propagating low-frequency components of the signal.

The first forerunner was initially analyzed by Sommerfeld [14]. He showed that it can be expressed in terms of the Bessel function J_1 with the argument proportional to $\sqrt{zt}$, where z and t are the propagation depth and time, respectively. The notion of the second forerunner was introduced by Brillouin [1, 2]. He expressed it in terms of the Airy function Ai. Both Sommerfeld and Brillouin restricted their analysis to the case of linearly-polarized pulses propagating in a single-resonance Lorentz medium. Over the years, their results were generalized and improved significantly [8, 9, 13]. The traditional way of the Fourier analysis and synthesis was usually utilized to arrive at the resulting time-dependent expressions.

Recently, new time-domain methods to analyze the second forerunner in unbounded, temporally dispersive, simple [6] or complex [3] media were suggested. They are based on parabolic (noncausal) approximations to the hyperbolic integro-differential equations for the right- and left-going electromagnetic field components. Working with an unbounded medium implies performance of measurements inside the material, which is usually a difficult task. It is much easier to measure the fields in vacuum at the interfaces of a finite slab made of the material in question. In the present article, the scattering kernels for a temporally dispersive, simple slab are analyzed. The second forerunner approximations for the transmission and the

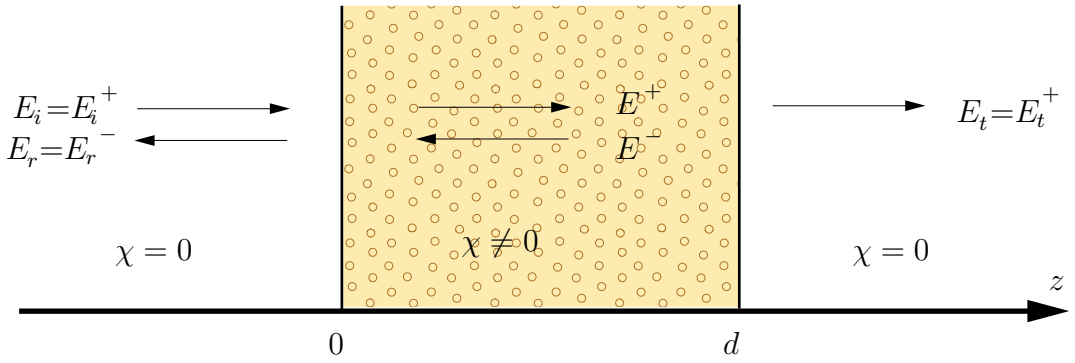

Figure 1: The geometry of the problem.

reflection kernels are derived. Note that first forerunners in temporally dispersive slabs were treated in Ref. 11.

The outline of the present article is as follows. In Section 2, notation and basic equations are presented. In Section 3, the dispersive wave splitting is introduced and the dynamics of the split fields is derived. The reflection and the transmission kernels at normal incidence for a temporally dispersive, simple slab are obtained in Section 4 and they are approximated asymptotically with respect to the slowly varying components (second forerunner approximation) in Section 5. In Section 6, the analytic and asymptotic expressions are tested numerically for two well-known dispersion models. The low frequency components of the numerical values of the scattering kernels are utilized in Section 7 to reconstruct the first few susceptibility moments of the medium. Finally, in Section 8, conclusions are drawn.

Note, that many of the results summarized in Sections 2–4 can be found in Refs. 6 and 12.

2 Basic equations

Throughout this paper, scalars are typed in italic style, vectors in italic boldface style, and dyadics in Roman boldface style. The speed of light in vacuum is c_0 and the intrinsic impedance of vacuum η_0. The source-free Maxwell equations are

$$\begin{cases} \nabla \times \boldsymbol{E}(\boldsymbol{r},t) = -\partial_t \boldsymbol{B}(\boldsymbol{r},t), \\ \nabla \times \boldsymbol{H}(\boldsymbol{r},t) = \partial_t \boldsymbol{D}(\boldsymbol{r},t). \end{cases} \tag{2.1}$$

All fields are assumed to be initially quiescent. This means that they all are zero before a certain time t, say $t = 0$.

The constitutive relations of a temporally dispersive, nonmagnetic, simple (linear, homogeneous, and isotropic) medium in the absence of an optical response are [5]

$$\begin{cases} c_0\eta_0 \boldsymbol{D}(\boldsymbol{r},t) = \boldsymbol{E}(\boldsymbol{r},t) + (\chi * \boldsymbol{E})(\boldsymbol{r},t) \\ c_0 \boldsymbol{B}(\boldsymbol{r},t) = \eta_0 \boldsymbol{H}(\boldsymbol{r},t), \end{cases} \tag{2.2}$$

where $\chi(t)$ is the susceptibility kernel of the medium. The asterisk $(*)$ denotes temporal convolution:

$$(\chi * \boldsymbol{E})(\boldsymbol{r}, t) = \int_{-\infty}^{t} \chi(t - t')\boldsymbol{E}(\boldsymbol{r}, t')\, dt'.$$

Due to causality, the kernel $\chi(t)$ vanishes for $t < 0$. Furthermore, it is supposed to be smooth and bounded for $t > 0$.

In this paper, linearly polarized plane wave propagation through a temporally dispersive, isotropic slab is investigated, see Figure 1. Only the case of the normal incidence is treated, *i.e.*, the fields depend on depth z only. Suppose that the electromagnetic fields can be written as

$$\begin{cases} \boldsymbol{E}(\boldsymbol{r}, t) = \boldsymbol{e}_x E(z, t) \\ \boldsymbol{H}(\boldsymbol{r}, t) = \boldsymbol{e}_y H(z; t), \end{cases}$$

where $\boldsymbol{e}_x$ and $\boldsymbol{e}_y$ are the unit vectors in x and y directions, respectively. Inside the slab, the Maxwell equations (2.1) together with the constitutive relations (2.2) give

$$c_0 \frac{\partial}{\partial z} \begin{pmatrix} E \\ -\eta_0 H \end{pmatrix} = \frac{\partial}{\partial t} \left\{ \begin{pmatrix} 0 & 1 \\ 1 + \chi * & 0 \end{pmatrix} \begin{pmatrix} E \\ -\eta_0 H \end{pmatrix} \right\}, \qquad 0 < z < d. \tag{2.3}$$

3 Wave splitting

The dispersive wave splitting suggested by Rikte [12] and used in, *e.g.*, Refs. 4, 6 is now adopted. Wave splitting is the change of the dependent vector field variables, such that the new variables, say $E^{\pm}(z, t)$, represent the right- and left-going field components in the medium. Introduce [6, 12]

$$\begin{cases} E^+ = \dfrac{1}{2}\left(E + (1 + Z*)\eta_0 H\right) \\ E^- = \dfrac{1}{2}\left(E - (1 + Z*)\eta_0 H\right). \end{cases} \tag{3.1}$$

The inverse transformation is given by

$$\begin{cases} E = E^+ + E^- \\ \eta_0 H = (1 + N*)(E^+ - E^-). \end{cases} \tag{3.2}$$

In the expressions above, the intrinsic impedance kernel $Z(t)$ and the refractive kernel $N(t)$ vanish for $t < 0$ and are well-behaved for $t > 0$. Furthermore, $N(t)$ is the resolvent of $Z(t)$, *i.e.*,

$$N(t) + Z(t) + (N * Z)(t) = 0 \tag{3.3}$$

The aim of the dispersive wave splitting is to decouple the Maxwell equations. Differentiating (3.1) with respect to z, using (2.3) and (3.2), and demanding decoupled equations for E^+ and E^- lead to the following equation for the kernel $N(t)$:

$$2N(t) + (N * N)(t) = \chi(t). \tag{3.4}$$

This is a nonlinear Volterra integral equation of the second kind which is known to be uniquely solvable. The equations for the split fields read

$$(c_0\partial_z \pm \partial_t)E^\pm = \mp\partial_t N * E^\pm, \qquad 0 < z < d. \tag{3.5}$$

Therefore, the split fields E^+ and E^- represent right- and left-going fields, respectively, both inside and outside the slab. Coupling between E^+ and E^- occurs only at the interfaces ($z = 0$ and $z = d$).

4 Reflection and transmission kernels for the slab

In this section, formulas for the transmission and the reflection kernels for a temporally dispersive, simple slab are obtained in a simple heuristic way. For a mathematically rigorous derivation see Ref. 12.

First, the reflection and the transmission kernels for a temporally dispersive half-space are obtained. Consider a plane wave, E, $\eta_0 H$, normally incident on a dispersive half-space $z > 0$ with the refractive kernel $N(t)$. In terms of the split fields, the situation outside the slab is as follows: the incident and the transmitted fields have only right-going components and the reflected field has only left-going component, *i.e.*,

$$E_i = E_i^+ = \frac{E_i + \eta_0 H_i}{2}, \qquad E_t = E_t^+ = \frac{E_t + (1 + Z*)\eta_0 H_t}{2}, \qquad E_r = E_r^- = \frac{E_r - \eta_0 H_r}{2}$$

The boundary conditions imply that

$$E_i + E_r = E_t, \qquad\qquad H_i + H_r = H_t. \tag{4.1}$$

The transmission and the reflection kernels for a dispersive half-space are defined as

$$E_t^+ = (1 + T_0*)E_i^+, \qquad\qquad E_r^- = R_0 * E_i^+, \tag{4.2}$$

respectively. Using these definitions, the boundary conditions (4.1), and the relations (3.2) one obtains

$$R_0(t) = -\left(\left(1 + \frac{N}{2}*\right)^{-1}\frac{N}{2}\right)(t), \qquad\qquad T_0(t) = R_0(t). \tag{4.3}$$

In the same way one can define the transmission and the reflection kernels, $T_1(t)$ and $R_1(t)$, respectively, viewed from the dispersive medium, *i.e.*, for the case when a

plane wave propagating in a dispersive half-space is incident on an interface between dispersive and nondispersive half-spaces. Calculations similar to the ones above show that

$$R_1(t) = \left(\left(1 + \frac{N}{2} * \right)^{-1} \frac{N}{2} \right)(t) = -R_0(t), \qquad T_1(t) = R_1(t).$$

Now consider a plane wave propagating in a dispersive medium. The split fields E^+ and E^- satisfy the Maxwell equations (3.5). The solution to (3.5) can be expressed in terms of the propagator operator [12]

$$E^{\pm}\left(z_2, t \pm (z_2 - z_1)/c_0\right) = \mathcal{P}(\pm(z_2 - z_1))E^{\pm}(z_1, t),$$

where

$$\begin{aligned} \mathcal{P}(z) &= \exp\left(-\frac{z}{c_0} \partial_t N * \right) = \exp\left(-\frac{z}{c_0} N(0) \right) \exp\left(-\frac{z}{c_0} N' * \right) \\ &= Q(z)(1 + P(z;\cdot) *). \end{aligned} \tag{4.4}$$

The wave-front propagator $Q(z)$ and the propagator kernel $P(z;t)$ in (4.4) are given by [6]

$$\begin{cases} Q(z) = \exp\left(-\dfrac{z}{c_0} N(0) \right) \\ P(z;\cdot) * = \exp\left(-\dfrac{z}{c_0} N' * \right) - 1 = \displaystyle\sum_{k=1}^{\infty} \frac{1}{k!} \left(\frac{-z}{c_0} \right)^k (N' *)^k. \end{cases} \tag{4.5}$$

Prime in the expressions above denotes the classical time derivative. The propagator kernel $P(z;t)$ satisfies the following Volterra integral equation of the second kind, which can be used to calculate $P(z;t)$ numerically [3, 6]:

$$tP(z;t) = -\left(F(\cdot) * P(\cdot) \right)(t) - F(t), \qquad F(t) = \frac{z}{c_0} t N'(t). \tag{4.6}$$

Now consider a dispersive slab with the refractive kernel $N(t)$ occupying the region $0 < z < d$. Suppose that a plane wave propagating in z-direction impinges normally on the slab at time $t = 0$. The wave is transmitted and reflected at the interface $z = 0$. Note that during the first round trip ($0 < t < 2d/c_0$), there is only right-going field component at $z = 0+$, because the wave splitting is perfect (*i.e.*, right- and left-going components are not coupled) and the reflected wave from the second interface ($z = d$) has not yet arrived. Therefore, the total reflected field at $z = 0-$ for $0 < t < 2d/c_0$ is $E_r^-(t) = (R_0 * E_i^+)(t)$. The transmitted wave propagates through the slab and at time $t = d/c_0$ the wave front reaches the second interface ($z = d$), where the wave is transmitted and reflected again. The total electric field at $z = d+$ for time $0 < t < d/c_0$ is zero and for $d/c_0 < t < 3d/c_0$ (the second reflection from the interface $z = 0$ has not arrived at the point $z = d-$) it is

$$E_t(t) = E_t^+(t) = ((1 + T_1 *)\mathcal{P}(d)(1 + T_0 *)E_i^+)(t - d/c_0).$$

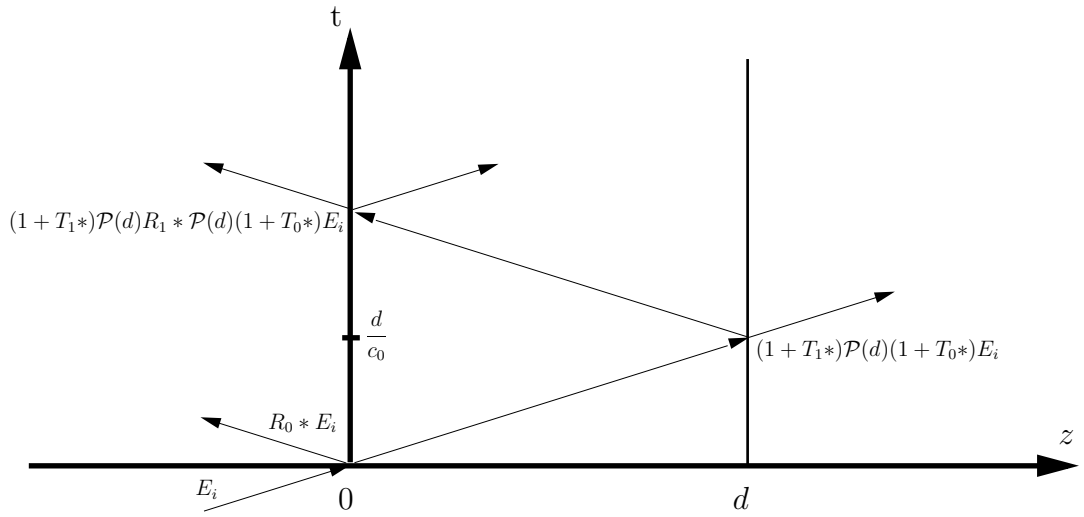

Figure 2: Reflection diagram.

The reflected wave propagates back through the slab and at time $t = 2d/c_0$ reaches the interface $z = 0$ and is reflected and transmitted one more time. So, for $0 < t < 4d/c_0$, the reflected field at $z = 0-$ can be written as

$$E_r(t) = E_r^-(t) = (R_0 * E_i^+)(t) + (1 + T_1*)\mathcal{P}(d)R_1 * \mathcal{P}(d)(1 + T_0*)E_i^+(t - 2d/c_0).$$

This is illustrated in the reflection diagram in Figure 2. So, finally, the transmission and reflection kernels for the slab, which are defined as

$$E_t^+(d+, t + d/c_0) = (Q(d) + T*)E_i^+(0-, t), \qquad E_r^-(0-, t) = R * E_i^+(0-, t),$$

are given by

$$\begin{array}{ll} Q(d)\delta(t) + T(t) = \mathcal{P}(d)(1 - R_0 * R_0)(t), & 0 < t < 2d/c_0, \\ R(t) = R_0(t) + \mathcal{P}(2d)\big((1 - R_0 * R_0*)R_0\big)(t - 2d/c_0), & 0 < t < 4d/c_0, \end{array} \tag{4.7}$$

where the commutative properties of the scattering and propagator operators were used as well as the fact that $\mathcal{P}^2(z) = \mathcal{P}(2z)$. The expressions for the scattering kernels in (4.7) can be easily generalized to be valid for other times t: one just has to take into account more reflections at the interfaces. However, for the purposes of the present paper, the formulas (4.7) are sufficient. In Ref. 12, the reader can find expressions for the scattering kernels of a slab valid for all times.

5 Second forerunner approximation

In this section, time-domain techniques [6] is used to obtain the approximation of the scattering kernels with respect to the slowly varying components.

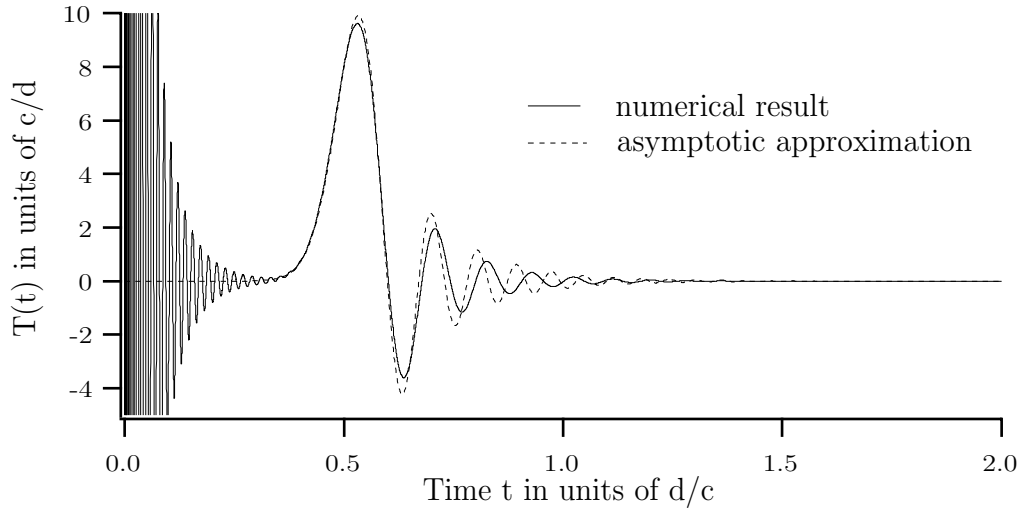

Figure 3: The transmission kernel $T(t)$ for a Lorentz slab. The slab is $10^{-6}\,\mathrm{m}$ thick and the material parameters are $\omega_p = \sqrt{20}\cdot 10^{16}\,\mathrm{s}^{-1}$, $\omega_0 = 4\cdot 10^{16}\,\mathrm{s}^{-1}$, and $\nu = 56\cdot 10^{14}\,\mathrm{s}^{-1}$.

First, approximate convolution with the susceptibility kernel as [6]

$$\chi* = \sum_{k=0}^{\infty} \chi_{k+1}\frac{d^k}{dt^k} \approx \sum_{k=0}^{2} \chi_{k+1}\frac{d^k}{dt^k}, \tag{5.1}$$

where the moments are

$$\chi_k = \frac{(-1)^{k-1}}{(k-1)!}\int_0^\infty t^{k-1}\chi(t)\,dt.$$

The refractive kernel $N(t)$ and the reflection kernel $R_0(t)$ are approximated in a similar way with the moments n_k and r_k, respectively. Having calculated the moments χ_k one can easily obtain n_k by substituting the expansions for $\chi*$ and $N*$ (see the first equality in (5.1)) into (3.4) and balancing the coefficients in front of the time derivatives of all orders. Similarly, using the expansions for $N*$ and R_0* in (4.3), the moments r_k can be obtained. For $k = 1, 2, 3$, one has

$$\begin{aligned} &n_1 = \sqrt{1+\chi_1} - 1, \quad n_2 = \frac{\chi_2}{2(1+n_1)}, \quad n_3 = \frac{\chi_3 - n_2^2}{2(1+n_1)}, \\ &r_1 = -\frac{n_1}{2+n_1}, \quad r_2 = -\frac{n_2 + r_1 n_2}{2+n_1}, \quad r_3 = -\frac{n_3 + n_2 r_2 + n_3 r_1}{2+n_1}. \end{aligned} \tag{5.2}$$

Introducing the approximation for $N(t)$ into (4.4) gives the second forerunner approximation to the propagator operator (see Ref. 6 for the details):

$$\mathcal{P}(z) \approx P_B(z;\cdot)* = \exp\left(\frac{n_2^3}{27n_3^2}\frac{z}{c} - \frac{n_2}{3n_3}\left(t - t_1(z)\right)\right)\frac{Ai\left(\mathrm{sign}(n_3)\frac{(t-t_1(z))}{t_3(z)}\right)}{t_3(z)}*, \tag{5.3}$$

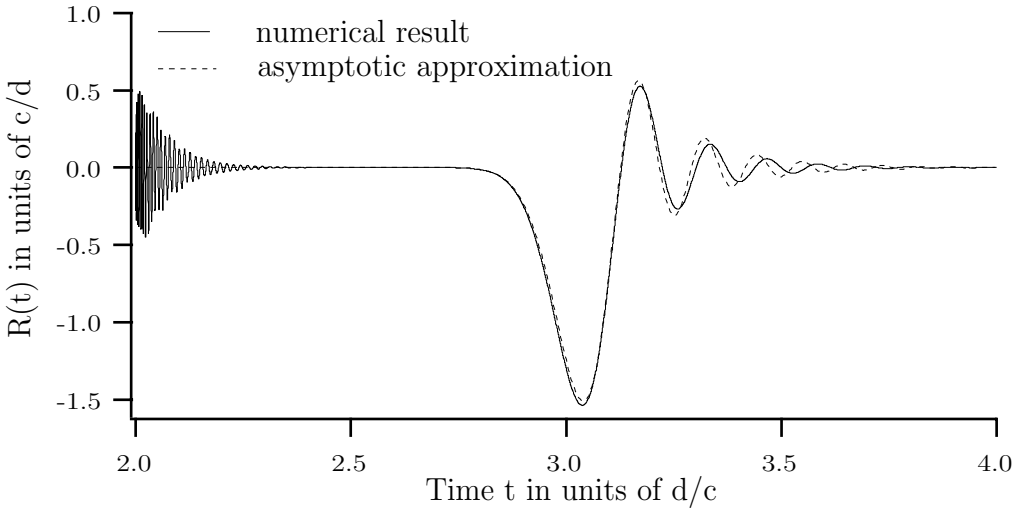

Figure 4: The reflection kernel $R(t)$ for a Lorentz slab during the second round trip. For medium parameters, see caption of Figure 3.

where the index "B" stands for "Brillouin" and

$$t_1(z) = \left(n_1 - \frac{n_2^2}{3n_3}\right)\frac{z}{c}, \qquad t_3(z) = \left(\frac{3|n_3|z}{c}\right)^{\frac{1}{3}}.$$

Improved approximations to the propagator operator containing convolutions of the hyper-Airy functions can be obtained, see Refs. 6 and 3.

Introducing (5.3) and the approximation for $R_0(t)$ into the representations (4.7) give the second forerunner approximations to the scattering kernels. The first term in the second equation in (4.7) is omitted because it does not contain the propagator $\mathcal{P}(z)$ which is fundamental in the suggested approximation. The result is

$$\begin{aligned} T(t) &\approx \Big(1 - r_1^2 - 2r_1r_2\partial_t - (2r_1r_3 + r_2^2)\partial_t^2 - 2r_2r_3\partial_t^3 - r_3^2\partial_t^4\Big) P_B(d;t) \\ R(t) &\approx \Big((r_1 - r_1^3) + (r_2 - 3r_1^2r_2)\partial_t + (r_3 - 3r_1r_2^2 - 3r_1^2r_3)\partial_t^2 - (6r_1r_2r_3 + r_2^3)\partial_t^3 \\ &\qquad - (3r_1r_3^2 + 3r_2^2r_3)\partial_t^4 - 3r_2r_3^2\partial_t^5 - r_3^3\partial_t^6\Big) P_B(2d; t - 2d/c_0). \end{aligned} \tag{5.4}$$

Using the well-known Airy equation, the approximations to the scattering kernels can be expressed as an algebraic combination of the exponential function, the Airy function, and its first derivative. The explicit expressions are easily obtained but are too lengthy to be presented in the paper. The main advantage with these expressions is that they are computationally cheap, *i.e.*, one does not need large computer capacities to be able to compute them.

6 Numerical example

In this section, the general expressions derived above are applied to two different material models and subjected to numerical evaluation.

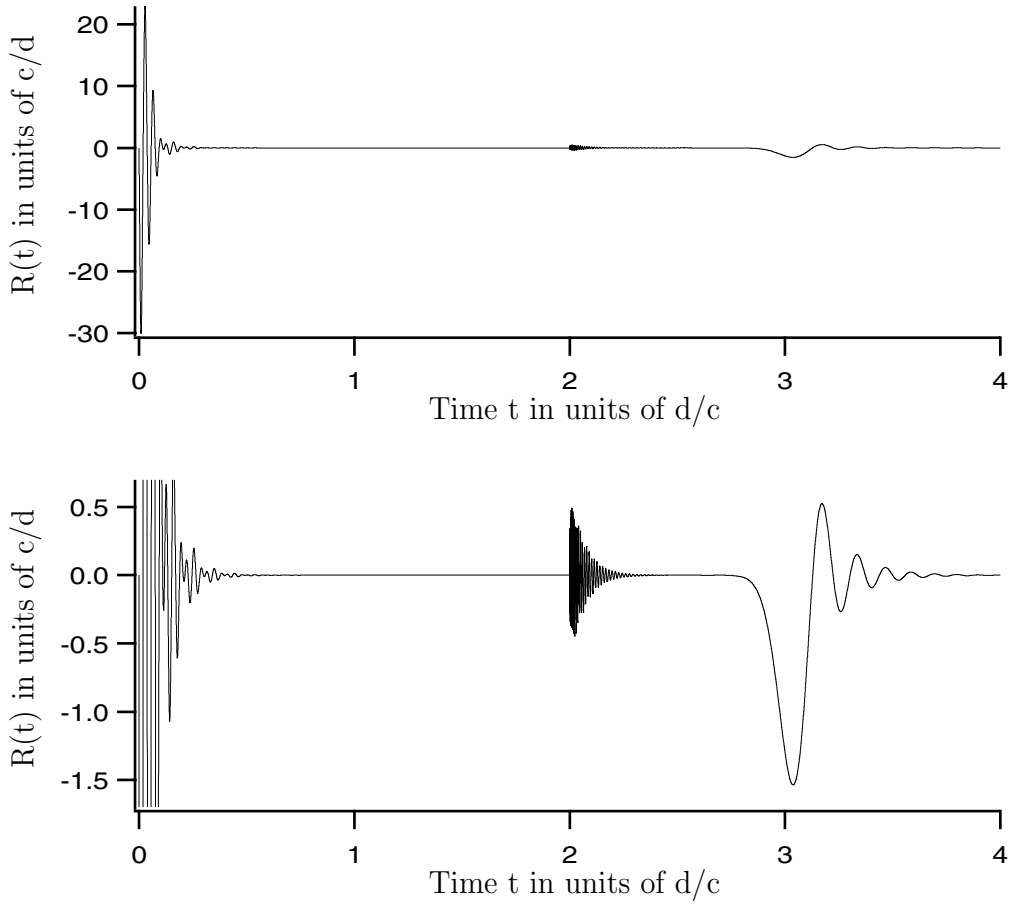

Figure 5: The reflection kernel $R(t)$ for a Lorentz slab during the first and the second round trips in two different scales. For medium parameters, see caption of Figure 3.

The numerical results are obtained by the following procedure. First, use (3.4) to calculate the refractive kernel. Then, solve (4.6) to obtain the propagator kernel $P(z;t)$ and use (4.5) to obtain the wave-front propagator. After that, calculate the reflection kernel for the dispersive half-space (4.3), and, finally, substitute the results into the representations (4.7). The approximations are obtained by first calculating the moments χ_k, n_k, and r_k and then using (5.4).

The results are presented in Figures 3–8. Note that time t in all the figures is the wave-front time, *i.e.*, $t = 0$ at $z = z_0$ when the wave front reaches the point $z = z_0$. It is given in units of d/c, while the amplitude is in units of c/d. The numerical and asymptotic results for the reflection kernel are compared with each other only for the second round trip ($2d/c < t < 4d/c$) because no second forerunner phenomena can be noticed during the first round trip (the propagator operator $\mathcal{P}(z)$ which forms the basis of the approximation is not contained in the expression for the reflection kernel during the first round trip).

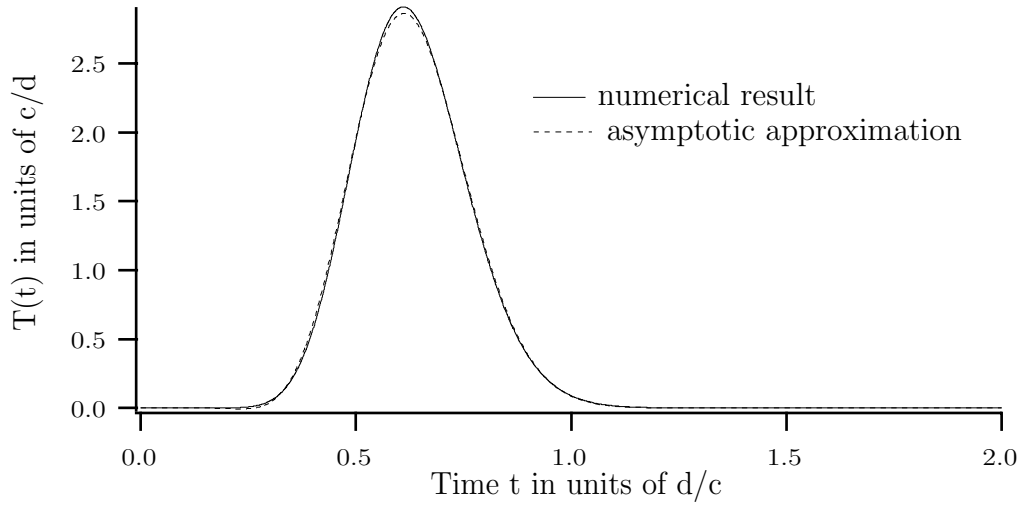

Figure 6: The transmission kernel $T(t)$ for a Debye slab. The slab is 1 m thick and the material parameters are $\alpha = 3 \cdot 10^{10}\,\mathrm{s}^{-1}$ and $\beta = 1.8 \cdot 10^{10}\,\mathrm{s}^{-1}$.

6.1 Lorentz medium

Suppose that the susceptibility kernel $\chi(t)$ for the material of the slab can be described by a single-resonance Lorentz model (*e.g.*, solids at infra-red or optical frequencies) [7]:

$$\chi(t) = \frac{\omega_p^2}{\nu_0} \sin(\nu_0 t) \exp\Big(-\frac{\nu}{2}t\Big) H(t),$$

where ω_0, ω_p, and ν are the harmonic, plasma, and collision frequencies of the medium, respectively, $\nu_0 = \sqrt{\omega_0^2 - \nu^2/4}$, and $H(t)$ is the Heaviside step function. For this model, the moments χ_1, χ_2, χ_3 are (*cf.* Ref. 6)

$$\chi_1 = \frac{\omega_p^2}{\omega_0^2}, \quad \chi_2 = -\frac{\nu\omega_p^2}{\omega_0^4}, \quad \chi_3 = -\frac{\omega_p^2(\omega_0^2 - \nu^2)}{\omega_0^6}.$$

The moments n_1, n_2, n_3 and r_1, r_2, r_3 are given by (5.2). In Figures 3 and 4, the transmission and the reflection kernels for a slab of Lorentz material are presented. The solid line represents the numerical results while the dashed line the asymptotic approximation. The slab is 10^{-6}m thick and the material is characterized by the following parameters: $\omega_p = \sqrt{20} \cdot 10^{16}\,\mathrm{s}^{-1}$, $\omega_0 = 4 \cdot 10^{16}\,\mathrm{s}^{-1}$, and $\nu = 56 \cdot 10^{14}\,\mathrm{s}^{-1}$. Note that the same material parameters were used in Refs. 4 and 6. The numerical values for the reflection kernel for the first two round trips can be found in Figure 5.

The transmission kernel for the slab does not differ much from the propagator kernel of the medium, $\mathcal{P}(d)$ (*cf.* [6, Figure 3]): the two transmissions through the interfaces do not change the signal considerably. The reflection kernel is, however, interesting to analyze. For the second round trip it is approximately equal to (see (4.7) and (4.4) and use the fact that for Lorentz media $Q(z) = 1$)

$$\Big(R_0 * (1 + P(2d;\cdot)\Big)\Big(t - \frac{2d}{c_0}\Big) = \Big(R_0 + R_0 * P(2d;\cdot)\Big)\Big(t - \frac{2d}{c_0}\Big), \qquad \frac{2d}{c_0} < t < \frac{4d}{c_0} \quad (6.1)$$

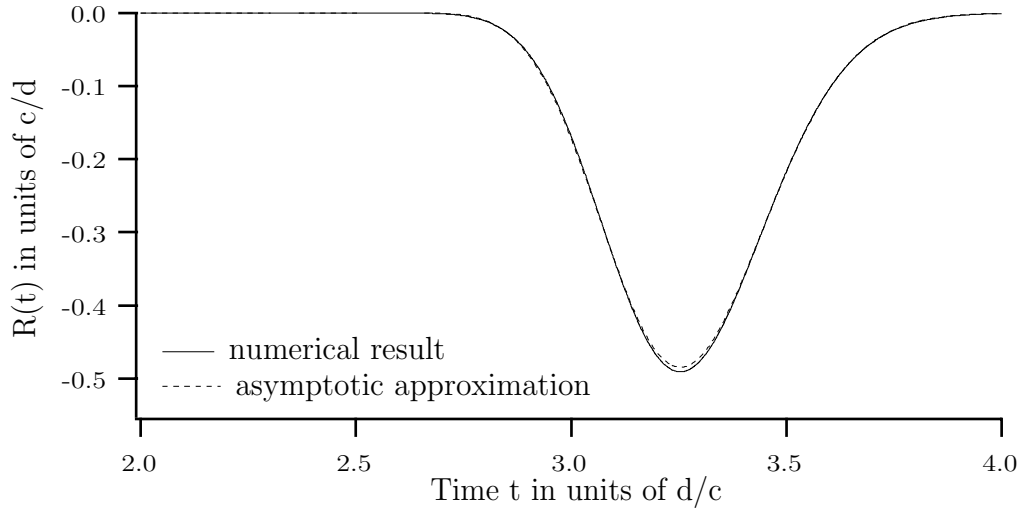

Figure 7: The reflection kernel $R(t)$ for a Debye slab during the second round trip. For medium parameters, see caption of Figure 6.

(again: the transmissions through the interfaces do not have vital influence on the signal). A quick glance at the expression above, gives the conclusion that the behavior of the reflection kernel at the beginnings of the first and the second round trips must be similar, because the term $R_0(t - 2d/c_0)$ seems to give the dominant contribution to the kernel R at the beginning of the second round trip (recall that during the first round trip, $R(t) = R_0(t)$). However, this is not the case, see Figure 5. The low amplitude of the oscillations at the beginning of the second round trip may be explained in the following way. The propagation kernel $P(z;t)$ for a dispersive Lorentz material for sufficiently large z can be written as a sum $P_1(z;t) + P_2(z;t)$, where the first term represents rapidly oscillating components which are usually characterized by very high amplitudes and the second term represents slowly varying components of the kernel. The kernel $P_1(z;t)$ can be approximated using first forerunner approximation [6, 10]. The kernel $P_2(z;t)$ can be approximated by the procedure outlined above. As was mentioned in Ref. 10, for large propagation depths (*i.e.*, large z) the first forerunner kernel tends to the Dirac delta function $-\delta(t)$. The distance $z = 2 \cdot 10^{-6}$ m is large in the optical domain. So the term $R_0 * P_1(2d;\cdot)$ in (6.1) nearly cancels R_0. This is clearly demonstrated by Figure 5.

6.2 Debye medium

Now suppose that the susceptibility kernel $\chi(t)$ of the slab satisfies the Debye model (*e.g.*, polar liquids at microwave frequencies) [7]

$$\chi(t) = \alpha e^{-\beta t} H(t),$$

where α is a frequency and $1/\beta$ the relaxation time. The susceptibility moments are then given by

$$\chi_k = (-1)^{k-1} \alpha \beta^{-k}, \qquad k = 1, 2, 3,$$

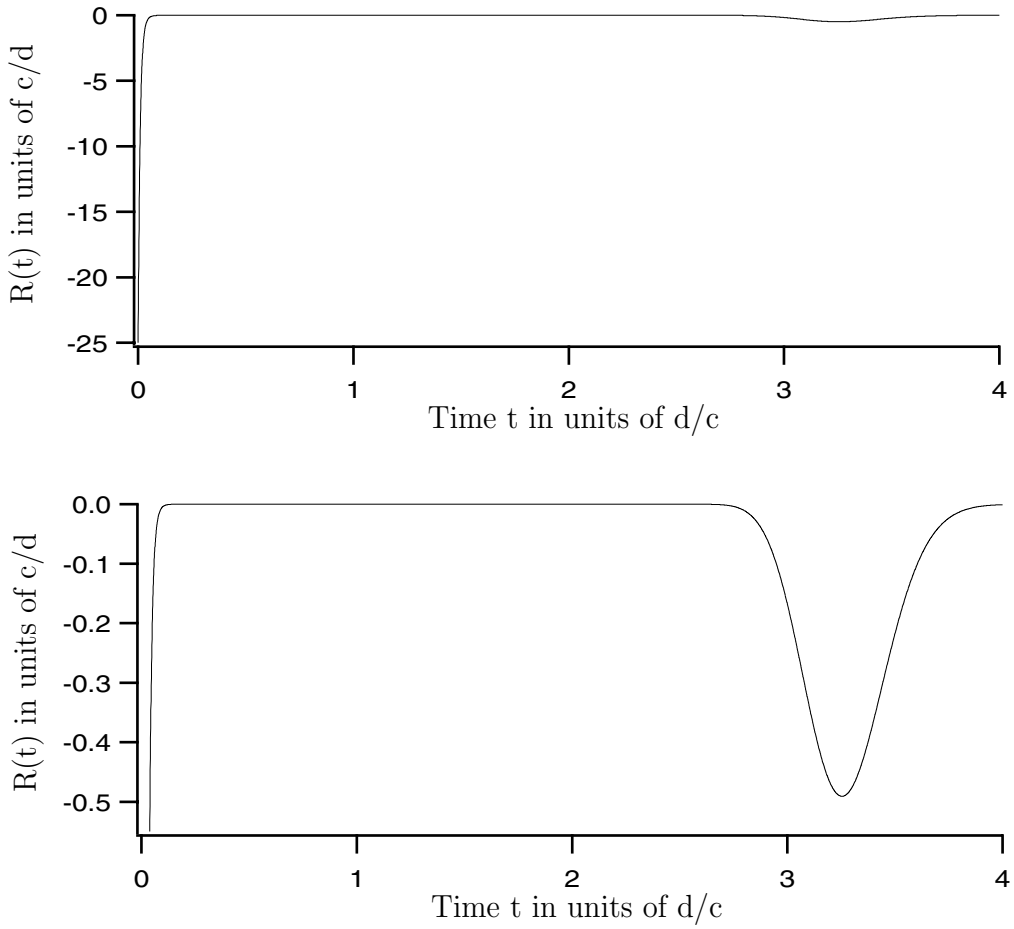

Figure 8: The reflection kernel $R(t)$ for a Debye slab during the first and the second round trips in two different scales. For medium parameters, see caption of Figure 6.

and the moments n_1, n_2, n_3 and r_1, r_2, r_3 can be calculated from (5.2). In Figures 6 and 7, the transmission and the reflection kernels for a slab of Debye material are presented. The solid line represents the numerical results while the dashed line the asymptotic approximation. The slab is 1m thick and the material is characterized by the following parameters: $\alpha = 3 \cdot 10^{10}\,\mathrm{s}^{-1}$ and $\beta = 1.8 \cdot 10^{10}\,\mathrm{s}^{-1}$.

The numerical values for the reflection kernel for the first two round trips are depicted in Figure 8 in two different scales. The agreement between the numeric and the asymptotic results in Figures 6 and 7 is almost perfect.

7 Reconstruction of the susceptibility moments

The approximations (5.4) to the transmission and the reflection kernels for a dispersive slab contain only algebraic combinations of the exponential function, the Airy function Ai, and its first derivative: higher derivatives of Ai can be eliminated with the help of the well-known Airy equation, $Ai''(x) = xAi(x)$. The relatively simple

structure of these approximations suggests the possibility to use them to reconstruct susceptibility moments χ_k, $k = 1, 2, 3$, for an unknown slab from the transmission or the reflection kernels which are supposed to be known experimentally. Note that the moments χ_k are essentially the coefficients in the Taylor series for the Fourier transform of the susceptibility kernel $\chi(t)$. The problem of constructing a function from the coefficients in its Taylor series is known to be ill-posed.

Expressions (5.4) can be considered as two three-parameter families of functions. (Recall that the moments n_1, n_2, n_3 and r_1, r_2, r_3 can be expressed in χ_1, χ_2, χ_3 through (5.2).) The problem of finding the susceptibility moments for the slab can be formulated as the fitting problem: find the values of the parameters χ_k, $k = 1, 2, 3$, such that the expressions (5.4) describe (the slowly varying components of) the scattering kernels in the best possible way (*e.g.*, in the least-squares sense).

To exemplify this idea, the numerical values of the scattering kernels computed in Section 6 are now used to reconstruct the moments χ_k, $k = 1, 2, 3$. The procedure is as follows. First, the low-frequency components of the kernels are extracted. This is required only for the Lorentz material, because there are no highly oscillating components in the scattering kernels for the Debye medium, *cf.* Figures 6–8. For the Lorentz material, this can be accomplished by setting the transmission kernel equal to zero for $t < 0.35\ d/c$ and the reflection kernel equal to zero for $t < 2.5d/c$, see Figures 3 and 4. After that, a function of three variables, χ_1, χ_2, and χ_3, is defined by summing the squares of differences between the experimental values of the scattering kernel (say, the reflection kernel) and the approximation (5.4) at some time-points (the number of time-points in the examples presented in the tables below is 128). The final step is to minimize this function. For this purpose the function "*fmins*" in MATLAB 5.1 was utilized.

In the tables below, the results of the suggested procedure are presented.

Lorentz medium			
	χ_1	χ_2	χ_3
exact value	1.2500	$-1.3125 \cdot 10^{-3}$	$-6.8934 \cdot 10^{-5}$
reconstruction from the transmission kernel	1.2415	$-1.6388 \cdot 10^{-3}$	$-8.2110 \cdot 10^{-5}$
reconstruction from the reflection kernel	1.2469	$-1.4217 \cdot 10^{-3}$	$-7.6626 \cdot 10^{-5}$

Debye medium			
	χ_1	χ_2	χ_3
exact value	1.6667	$-2.7778 \cdot 10^{-2}$	$4.6296 \cdot 10^{-4}$
reconstruction from the transmission kernel	1.6655	$-2.6973 \cdot 10^{-2}$	$4.3449 \cdot 10^{-4}$
reconstruction from the reflection kernel	1.6681	$-2.7206 \cdot 10^{-2}$	$4.5949 \cdot 10^{-4}$

In the first rows of the tables, the exact values of the susceptibility moments for the

Lorentz and the Debye materials discussed in Section 6 are found. In the second rows, the moments reconstructed from the transmission data (transmission kernel $T(t)$) are given while the third row presents the moments reconstructed from the reflection data (the kernel $R(t)$). From the tables it follows that the reconstructed moments are closer to the exact ones for the Debye slab. This can be explained by the fact that the second forerunner approximations to the scattering kernels give better results for the Debye medium then for the Lorentz medium, *cf.* Figures 3, 4, 6, and 7, and the suggested method is based on these approximations.

8 Conclusion

This paper concerns electromagnetic pulse propagation in temporally dispersive, simple slabs. The analysis is performed using time-domain techniques. The second forerunner approximations to the transmission and the reflection kernels are obtained by extension of time-domain methods introduced in Ref. 6. The forerunners are expressed in terms of the Airy function, Ai. The numerical calculations are performed to obtain the exact (numerical) and the asymptotic values of the scattering kernels for two well-known dispersion models: the single-resonance Lorentz model and the Debye model. They show good agreement between the low-frequency components of the kernels and the second forerunner approximations. It should be mentioned that the approximations are computationally cheap: if it takes hours to compute the numerical values of the kernels it takes only seconds to get the second forerunner approximations.

Note also that in experiments with Lorentz materials, it is easier to view the second forerunner in the reflection data then in the transmission data due to the fact that the high amplitude oscillations present in the transmission kernel (the first forerunner) are absent (or significantly damped) in the reflection kernel, *cf.* Figures 4–5.

The slowly varying components of the scattering kernels can be used to reconstruct the first few susceptibility moments of the material by a least-squares fitting procedure. Mathematically this is equivalent to minimizing a certain function of several variables.

The analysis presented in this paper can be easily generalized to the case of bi-isotropic (or, more generally, bi-gyrotropic) materials. The complex time-dependent electromagnetic fields introduced in Ref. 3 can be then utilized.

Acknowledgment

The work reported in this paper is partially supported by a grant from the Swedish Research Council for Engineering Sciences, and its support is gratefully acknowledged.

References

[1] L. Brillouin. Über die Fortpflanzung des Lichtes in dispergierenden Medien. *Ann. Phys.*, **44**, 203–240, 1914.

[2] L. Brillouin. *Wave propagation and group velocity.* Academic Press, New York, 1960.

[3] I. Egorov and S. Rikte. Forerunners in bi-gyrotropic materials. Technical Report LUTEDX/(TEAT-7061)/1–27/(1997), Lund Institute of Technology, Department of Electromagnetic Theory, P.O. Box 118, S-211 00 Lund, Sweden, 1997.

[4] I. Egorov, A. Karlsson, and S. Rikte. Time-domain Green dyadics for temporally dispersive, simple media. *J. Phys. A: Math. Gen.*, **31**(14), 3219–3240, 1998.

[5] A. Karlsson and G. Kristensson. Constitutive relations, dissipation and reciprocity for the Maxwell equations in the time domain. *J. Electro. Waves Applic.*, **6**(5/6), 537–551, 1992.

[6] A. Karlsson and S. Rikte. The time-domain theory of forerunners. *J. Opt. Soc. Am. A*, **15**(2), 487–502, 1998.

[7] G. Kristensson. Direct and inverse scattering problems in dispersive media—Green's functions and invariant imbedding techniques. In R. Kleinman, R. Kress, and E. Martensen, editors, *Direct and Inverse Boundary Value Problems*, Methoden und Verfahren der Mathematischen Physik, Band 37, pages 105–119, Frankfurt am Main, 1991. Peter Lang.

[8] K. E. Oughstun and G. C. Sherman. Propagation of electromagnetic pulses in a linear dispersive medium with absorption (the Lorentz medium). *J. Opt. Soc. Am. B*, **5**(4), 817–849, 1988.

[9] K. E. Oughstun and G. C. Sherman. *Electromagnetic Pulse Propagation in Causal Dielectrics.* Springer-Verlag, Berlin Heidelberg, 1994.

[10] S. Rikte. *Propagation of transient electromagnetic waves in stratified bi-isotropic media and related inverse scattering problems.* PhD thesis, Lund Institute of Technology, Department of Electromagnetic Theory, P.O. Box 118, S-211 00 Lund, Sweden, 1994.

[11] S. Rikte. Sommerfeld's forerunner in stratified isotropic and bi-isotropic media. Technical Report LUTEDX/(TEAT-7036)/1–26/(1994), Lund Institute of Technology, Department of Electromagnetic Theory, P.O. Box 118, S-211 00 Lund, Sweden, 1994.

[12] S. Rikte. The Theory of the Propagation of TEM-Pulses in Dispersive Bi-isotropic Slabs. Technical Report LUTEDX/(TEAT-7040)/1–22/(1995), Lund Institute of Technology, Department of Electromagnetic Theory, P.O. Box 118, S-211 00 Lund, Sweden, 1995.

[13] S. Shen and K. E. Oughstun. Dispersive pulse propagation in a double-resonance Lorentz medium. *J. Opt. Soc. Am. B*, **6**(5), 948–963, 1989.

[14] A. Sommerfeld. Über die Fortpflanzung des Lichtes in dispergierenden Medien. *Ann. Phys.*, **44**, 177–202, 1914.